Growth, structuring and characterisation of all-oxide thin film devices prepared by pulsed laser deposition

Cillessen, J.F.M.; Wolf, R.M.; Giesbers, J.B.; Blom, P.W.M.; Grosse Holz, K.O.; Pastoor, E.

Published in:
Applied Surface Science

DOI:
10.1016/0169-4332(95)00548-x

Publication date:
1996

ELSEVIER

Applied Surface Science 96–98 (1996) 744–751

applied surface science

Growth, structuring and characterisation of all-oxide thin film devices prepared by pulsed laser deposition

J.F.M. Cillessen [a,*], R.M. Wolf [a], J.B. Giesbers [a], P.W.M. Blom [a], K.-O. Grosse-Holz [a,b], E. Pastoor [a,c]

[a] *Philips Research Laboratories, Prof. Holstlaan 4, 5656 AA Eindhoven, The Netherlands*
[b] *Institut für Werkstoffe der Elektrotechnik, RWTH Aachen, Germany*
[c] *Department of Applied Physics, University of Groningen, Groningen, The Netherlands*

Received 22 May 1995

Abstract

The combination of a variety of oxidic thin films in two materials systems is described. The first one focuses on the growth of $BaZrO_3$ on $SrTiO_3$ (both perovskites) and the use of these stacks as a substrate for the growth of magnetic ferrite spinel films. The second system shows the combination of oxidic conductors, ferroelectrics and semiconductors in all-oxide field effect devices. The control of stoichiometry for the ferroelectric used in this device (consisting of highly volatile components) as well as the improvement of thickness uniformity using off-axis PLD are discussed.

1. Introduction

The search for thin film applications of oxidic materials in future devices has made a big step forward by the improvement of thin film deposition techniques. Pulsed laser deposition (PLD) proves to be a useful tool in this context for the growth of stacks of oxidic layers, especially for multicomponent materials. Within the large variety of oxidic materials interesting combinations of compounds sharing the FCC oxygen sublattice structure are possible. The growth of oxides like high-T_c superconductor materials and ferroelectrics on MgO is well-known. Epitaxial growth of dissimilar oxides appears to be feasible even for materials showing a relatively large lattice mismatch. Another possible combination is that of perovskite and spinel crystal structures. They show an overlap of their oxygen sublattice unit cell in the 0.39–0.46 nm range. Such a combination offers possibilities for challenging applications since these oxides show a variety of functionalities like magnetism, electro-optics, conductivity, dielectricity and ferro-electricity.

In the first part of the paper some growth aspects concerning the epitaxy of oxides will be discussed. Materials described are the dielectric perovskite $BaZrO_3$ as well as the magnetic spinel $Mn_{0.6}Zn_{0.3}Fe(II)_{0.1}Fe(III)_2O_4$. After this, the growth of stoichiometric $Pb(Zr,Ti)O_3$ films is described, as used in the field effect device presented in the third section. The second part of this paper deals about the

* Corresponding author. Fax: +31-40 2743352; e-mail: cillessn@natlab.research.philips.com.

0169-4332/96/$15.00
SSDI 0169-4332(95)00548-X

improvement of thickness uniformity of PLD films using the off-axis technique.

2. Epitaxial oxidic films

2.1. Dielectric $BaZrO_3$ films

In order to study the relaxation behaviour of thin films, epitaxial $BaZrO_3$ films were grown on $SrTiO_3(100)$ substrates with thicknesses in the range from 1–53 nm. This set of both perfect cubic perovskites was chosen because of the large mismatch between these materials ($a = 0.419$ and 0.390 nm respectively). The pulsed laser deposition (PLD) technique was used and deposition parameters are listed in Table 1.

Conventional Θ–2Θ X-ray diffraction (XRD) of the $BaZrO_3$ layers showed only $(00l)$ reflections indicating textured or epitaxial growth. In-plane lattice parameters ($a_{\parallel}$) were determined and the epitaxial relation with the substrate unit cell was demonstrated using grazing incidence diffraction (GID) [1] with a set-up shown in Fig. 1. This technique is highly surface sensitive. Analyses show that the in-plane $BaZrO_3$ lattice cell parameters shift towards that of the substrate for ultra thin films (Fig. 2). Both in-plane lattice parameters showed the same value within the experimental error. Films with thicknesses > 4 nm appeared to be cubic: the lattice cell parameter was comparable with that of bulk $BaZrO_3$. Unfortunately the perpendicular latticeparameter of the thinnest sample could not be determined because of the low signal intensity in the Θ–2Θ XRD set-up. Given the in-plane lattice compression, an enlarged c-axis is expected.

Table 1
Experimental parameters for the deposition of various oxides

	$T_{deposition}$ (°C)	P_{oxygen} (mbar)
$BaZrO_3$	650°C (on oxides)	0.2
	605°C (on Si)	
$Mn_{0.6}Zn_{0.3}Fe_{0.1}Fe_2O_4$	600°C	10^{-3}
$Pb(Zr,Ti)O_3$	587°C	0.2
SnO_2: 300 ppm Sb	505°C	0.2
$SrRuO_3$	590–650°C	0.2
Excimer laser:	ArF ↔ 193 nm	
Pulswidth:	15 ns	
Repetition rate:	1–3 Hz	
Pulse-energy:	350 mJ	
Fluence:	5.2 J cm^{-2}	
Spotsize:	4.5 × 1.5 mm^2	

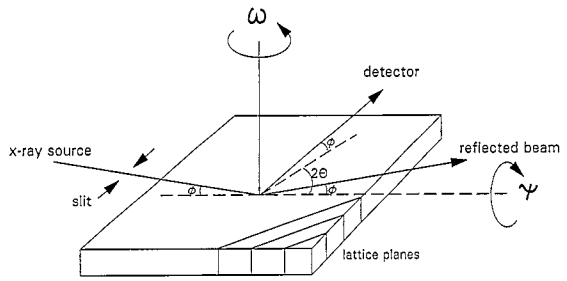

Fig. 1. Set-up for X-ray grazing incidence diffraction (GID).

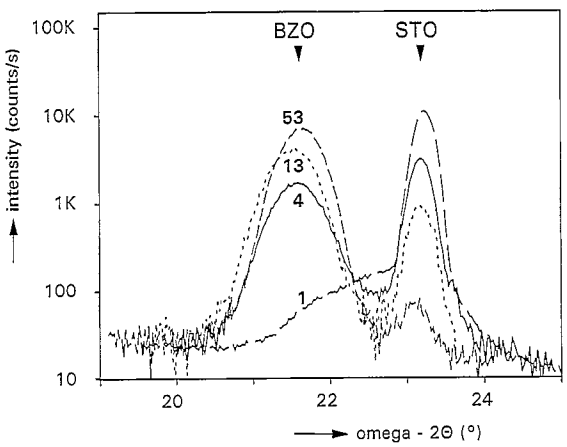

Fig. 2. Omega–2Θ scan (grazing incidence X-ray diffraction) showing a shift of the in-plane $BaZrO_3$ lattice parameter on a $SrTiO_3(100)$ substrate for ultra thin films (thicknesses shown are 1, 4, 13 and 53 nm).

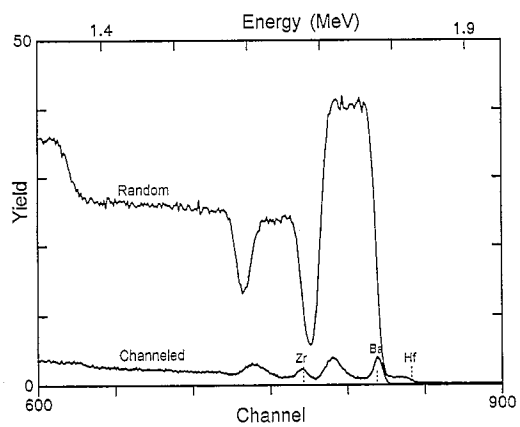

Fig. 3. Random and (100) channeled spectrum of $BaZrO_3$ film on $SrTiO_3(100)$.

Rutherford Backscattering Spectroscopy (RBS) analyses (Fig. 3) of these films show a perfect 1 : 1 cation stoichiometry within 3%. Minimum channeling yields of 2–2.5% demonstrate the epitaxial quality of the films. Deformation of the first unit cells as observed by GID were confirmed by RBS data: dechanneling only takes place in the interfacial area (for both the Ba as well as the Zr signal). The Hf signal observed in these spectra was always found as a $< 1\%$ impurity from our target. Hf is a common impurity in Zr compounds because of its chemical similarity. This also holds for our $Pb(Zr,Ti)O_3$ films. For both films, Hf is not expected to disturb structural properties: it fits on the B-site of the perovskite crystal structure and shows a perfect channeling characteristic as shown for the $BaZrO_3$ films.

In addition TEM was used to analyse thin $BaZrO_3$ films on $SrTiO_3(100)$. Selected area electron diffraction (SAED) in Fig. 4(a) again shows the epitaxial relation between substrate and film. The high resolution image shows that accommodation of the mismatch only takes place in the interfacial area. The amount of dislocations situated at the interface is given in Fig. 4(b). A 1 : 14 relation could be derived by averaging the results of a series of similar micrographs. This corresponds to the average mismatch

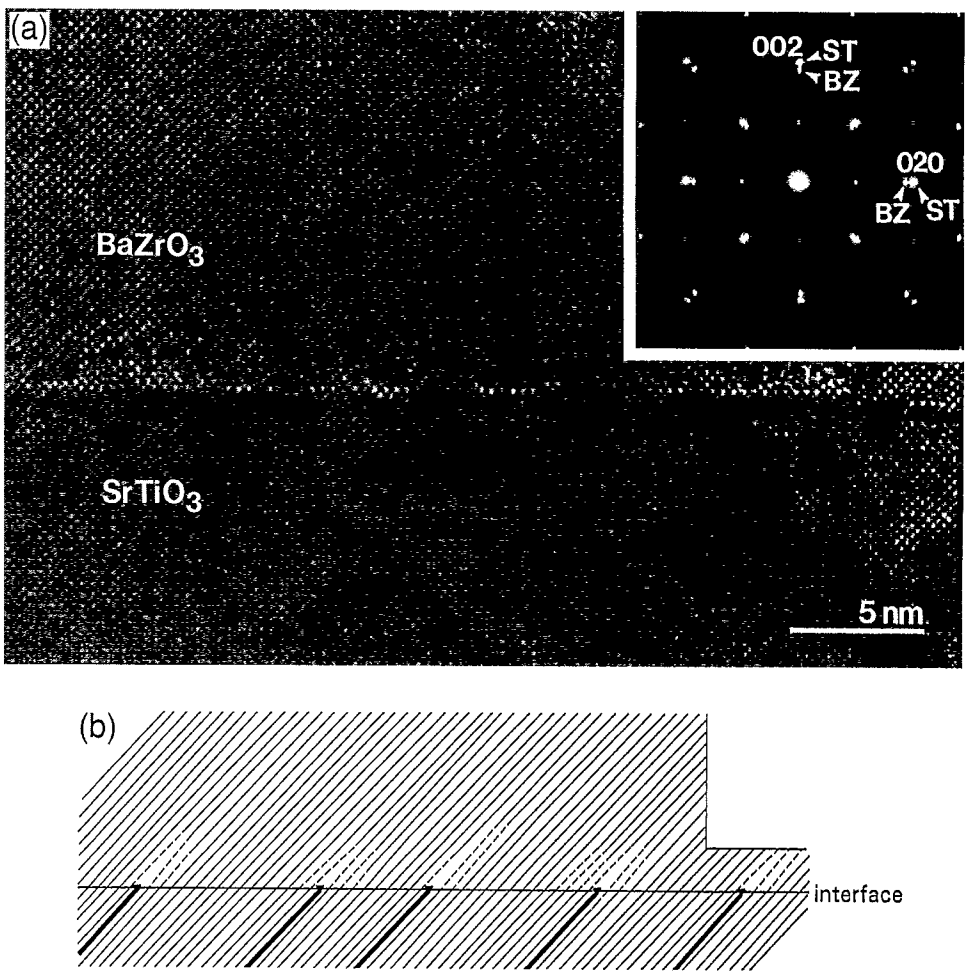

Fig. 4. (a) Cross-section TEM micrograph showing an epitaxial relation between $SrTiO_3$ and $BaZrO_3$: the amount of interfacial dislocations (1 in every 14 unit cells) corresponds to the average mismatch. (b) overlay for (a) showing the lattice planes and interfacial dislocations (marked by ▼). (A 1 : 1 transparency copy can be used as an overlay for the TEM micrograph of (a).)

between $BaZrO_3$ and $SrTiO_3$ which is defined as: $(\Delta a/a)_{av} = 2[(a_{BZO} - a_{STO})/(a_{BZO} + a_{STO})] \times 100\% = 7.17\%$.

2.2. Magnetic ferrite films

Manganese zinc ferrite (MZF) exhibits the spinel structure and is, amongst others, a well known soft magnetic material used in magnetic recording heads. For the study of intrinsic materials parameters epitaxial films were prepared. They have a more favourable microstructure since the number of grain boundaries is reduced. This for instance leads to a decrease of the coercive field strength H_c [2]. The growth of ferrite films has been subject to many studies during the last years by several research groups [3,4].

Deposition of MZF on bare $SrTiO_3(100)$ substrates resulted in mainly (111) oriented ferrite films (the most stable face for a spinel-type material). This indicates there is no driving force for epitaxy, most probably because of the large lattice mismatch ($(\Delta a/a)_{av} = 8.35\%$). Since the room temperature oxygen sublattice cell parameter of MZF is 0.848 nm, it shows a good fit to $BaZrO_3$ ($(\Delta a/a)_{av} = 1.2\%$). Deposition of MZF on relaxed $BaZrO_3$ layers (thickness 50 nm) on $SrTiO_3(100)$ substrates resulted in epitaxial spinel growth.

Epitaxial growth was also observed on (100) oriented spinel substrates of $MgAl_2O_4$ ($a = 0.808$ nm), but a serious interdiffusion of Mg into the ferrite lattice was found as analysed by SIMS. This diffusion was shown to take place at substrate temperatures above 400°C. $MgFe_2O_4$ however is not applicable for the purpose described, since it shows a much lower magnetisation (a factor of about 3 at room temperature [5]).

The best films in terms of rocking curve width and structural fit were deposited using similar conditions on Zn_2TiO_4 single crystals. These substrates have an almost perfect structural and lattice match (spinel, $a = 0.848$ nm). [1]

Magnetic analyses of all the layers (0.7 μm thickness) indicated a lowering of the magnetic coercive field strength (H_c) from 1.25 to 0.35 kA/m for the bare $SrTiO_3$ and $BaZrO_3$ coated $SrTiO_3$ substrates respectively. Films on Zn_2TiO_4 substrates showed the lowest value for H_c: 0.14 kA/m.

The effect of strain in magnetic materials is given by the magnetostriction constant λ (the fractional change of length upon an applied magnetic field). λ is dependent on the crystallographic orientation and λ_{100} for the chosen MZF composition [7] is $\sim -1 \times 10^{-5}$. Since in ferrites with λ values of $> |5 \times 10^{-6}|$ the magnetic performance is highly influenced by strain, this might explain why the bulkvalue for H_c is not obtained in our films. H_c for coarse grained MZF ceramics and single crystals is of the order of a factor 50 lower than our lowest reported value.

These results clearly demonstrate the influence of the difference in thermal expansion between the perovskite and the spinel structure on the magnetic properties of these layers. Thermal expansion coefficients of perovskites and spinels are about 7 and 70 ppm/K respectively. This means that the cubic ferrite unit cell builds up a tensile stress after growth during cooling down. In the case of a combination of two perovskites ($BaZrO_3$ deposited on $SrTiO_3$), where only the lattice mismatch plays a role, strain is restricted to the interfacial area. Relaxation of strain in the spinel-perovskite combination takes place over much larger distances. In fact, on the top side of a 0.25 μm ferrite film (on $BaZrO_3$ buffered $SrTiO_3$) analyses showed ferrite unit cells that were far from the cubic structure ($0.831 \times 0.831 \times 0.846$ nm analysed with GID).

These examples show that the (in this case) magnetic performance of the combination of different crystal structures is highly influenced by thermally induced strain.

2.3. Ferroelectric $PbZr_{1-x}Ti_xO_3$ films

During the growth of multicomponent thin films consisting of highly volatile constituents like $LiNbO_3$ ($Li_2O\uparrow$) or $PbZr_{1-x}Ti_xO_3$ ($PbO\uparrow$) stoichiometry may be lost during the deposition process. To obtain high quality ferroelectrics, the stoichiometry of $PbZr_{1-x}Ti_xO_3$ (PZT) films turns out to be very important. Deficiency of lead or oxygen will give rise to leakage currents.

[1] Zn_2TiO_4 single crystals were grown at the Philips Research Laboratory using the Bridgman–Stockbarger technique [6].

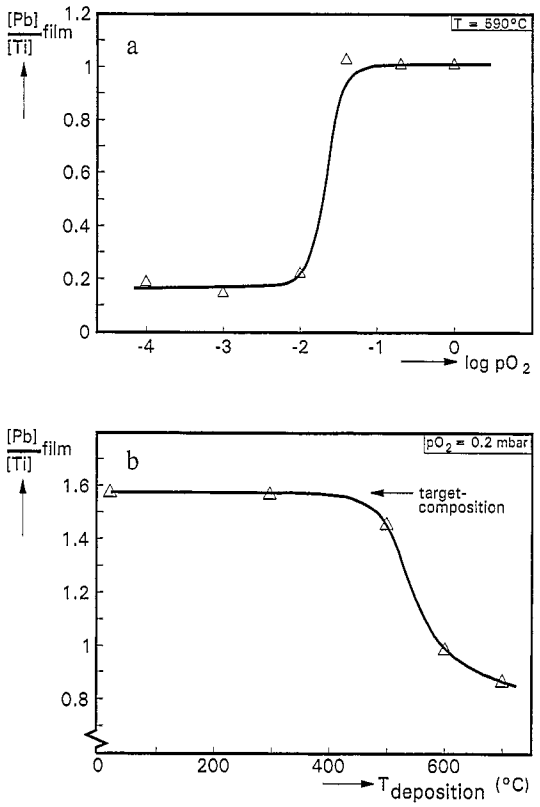

Fig. 5. (a) [Pb]/[Ti] stoichiometry of $PbTiO_3$ films versus temperature. (b) [Pb]/[Ti] stoichiometry of $PbTiO_3$ films versus oxygen pressure.

Proper growth of stoichiometric PZT films can only be carried out in a small window of deposition parameters because of the high volatility of Pb and PbO. This is the reason why PZT targets used for PLD are generally enriched with PbO. Ablation from such targets onto room temperature substrates show that the intrinsic ablation process is stoichiometric: films show the target stoichiometry (the sticking coefficient at room temperature is 1). However, deposition on substrates of 400°C or more show PbO desorption from the substrate surface. The dependence of the cation stoichiometry in the films as a function of deposition conditions is shown in Fig. 5(a) and (b). A high oxygen pressure is necessary to keep Pb in the oxidised state and to increase the sticking coefficient of PbO to the substrate surface. The ultimate composition of the films is determined by the balance between the rates of deposition, desorption and reaction ($PbO + TiO_2 + ZrO_2 \rightarrow PZT$).

For epitaxial films, a substrate temperature of at least 550°C is necessary, because a minimum surface mobility is required [8]. This temperature holds for deposition in O_2 gas. For more strongly oxidizing gases like N_2O, NO_2 or O_3 (also used for the deposition of high-T_c superconductors) or the use of laser excitation of the substrate surface [9], slightly lower deposition temperatures (−50°C) have been reported.

The influence of electrodes regarding the quality of contacts connecting ferroelectric oxides has been discussed in many papers [10,11]. The use of oxidic electrodes like $(La,Sr)CoO_3$ or $SrRuO_3$ provide the possibility of epitaxial growth because of their compatibility in terms of crystallographic structure [12,13]. This allows for chemically and mechanically stable stacks. The use of oxidic electrodes is not only favourable for epitaxial PZT layers: polycrystalline stacks were also shown to profit by the use of oxidic electrodes caused by the grain-epitaxial nature [12].

3. The off-axis PLD technique

Devices consisting of a variety of materials generally require the use of structuring techniques like wet or reactive ion etching (RIE) for pattern definition. One of the major requirements is the thickness uniformity of the layers. Especially devices consisting of a variety of oxidic materials are difficult to etch. Beside low RIE rates (of the order of a few nanometer per minute) these materials can often not be etched selectively. This means that the thickness uniformity of the different layers becomes an important factor, since the etching process is controlled by a predetermined etch-rate.

The use of PLD for the growth of complex oxidic materials has been demonstrated to be very successful. PLD however conventionally produces films with a significant thickness variation. This is mainly determined by the (Gaussian-tophat) energy distribution in the beam in commercially available excimer lasers. To circumvent this, off-axis PLD for the deposition of uniform films was investigated. In this technique, the substrate is off-centered from the ablation plume as proposed by Ianno et al. [14]. It offers the possibility to enlarge the area of uniform thickness in a relatively simple way. The intrinsic thick-

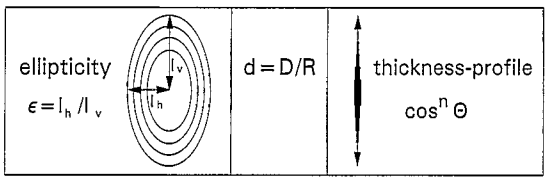

Fig. 6. The intrinsic thickness profile of PLD deposits is determined by a $\cos^n\theta$ distribution along the vertical axis of the deposit together with an ellipticity ϵ.

ness profile of the deposit (on a static substrate) has an elliptical form. It is described by two parameters: the thickness profile along the vertical axis of the deposit (a $\cos^n\Theta$ distribution [15]) in combination with the ellipticity ϵ, which is defined as the ratio of the horizontal and the vertical radius I_h/I_v of the deposit (see Fig. 6).

After off-setting the substrate centre from the ablation plume the thickness at position P on the substrate at radial distance r and spatial angle α (Fig. 7) can be calculated by the relation derived by Ianno:

$$T_P(\alpha, r) = \frac{A(\epsilon \cdot d)^n}{\left(\epsilon^2 d^2 + \epsilon^2 r^2 \cdot \sin^2\alpha + (r \cdot \cos\alpha - R)^2\right)^{n/2}}$$

where A is a normalisation factor corresponding to the maximum thickness in the centre of the plume, ϵ

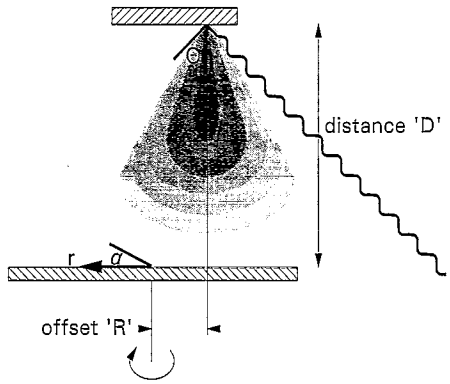

Fig. 7. Schematic set-up for the off-axis PLD technique showing the parameters necessary for thickness calculation for rotating substrates.

the ellipticity of the deposit, R the substrate offset from the centre of the laserplume and $d = D/R$ the distance ratio (in our case D was kept constant at 60 mm).

Integration $(0 \cdots \alpha \cdots \pi)$ of this equation generates the thickness profile for a rotating substrate. An example of such a simulated thickness profile is given in Fig. 8. For this simulation a range of d-values was used in combination with a $\cos^{11.5}\Theta$ distribution and an $\epsilon = 0.636$. These parameters were determined for (polycrystalline) $BaZrO_3$ films on Si using conditions given in Table 1. The distance ratio

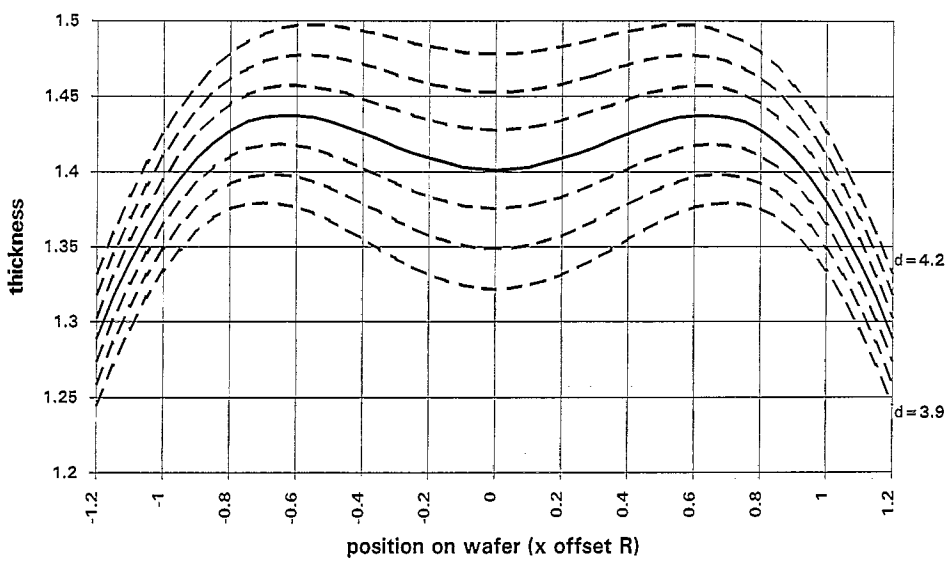

Fig. 8. Simulated thickness profile for a range of d-values ($d = D/R$). A $\cos^{11.5}\Theta$ distribution and ϵ of 0.636 were used as analysed for $BaZrO_3$ films deposited on Si (606°C, 0.2 mbar O_2).

value (d) representing the best uniformity is shown in Fig. 8 by the drawn line ($d = 4.05$). This corresponds to a thickness uniformity of roughly $\pm 1\%$ within an area of 30 mm diameter. Presently, the dependence of the cosine power 'n' and ellipticity 'ϵ' on pressure as well as the composition on large areas are under investigation.

4. Ferroelectric field effect device

The off-axis PLD technique and optimised deposition parameters for the growth of PZT films were applied for the preparation of the all-oxide ferroelectric field effect device shown in Fig. 9. This device consists of a combination of three types of oxidic materials: conductor, ferroelectric and semiconductor. $SrRuO_3$ was used as gate material (room temperature resistivity 4×10^{-4} Ω cm). The ferroelectric was $PbZr_{0.2}Ti_{0.8}O_3$, 300 ppm Sb doped SnO_2 was the source–drain semiconductor channel (room temperature charge carrier concentration 5×10^{17} cm^{-3}). [2] The ferroelectric $PbZr_{0.2}Ti_{0.8}O_3$ composition was chosen, because it is a good insulator and shows a steep hysteresis loop. In comparison with $PbTiO_3$, this composition does not show a large structural anisotropy, which would introduce a significant strain in the device upon cooling after growth.

Films were prepared using the conditions indicated in Table 1. After growth of an epitaxial layer of $SrRuO_3$ on $SrTiO_3(100)$, the sample was taken out of the vacuum and structured by means of Ar assisted reactive ion etching (RIE) with Ar/CHF_3. Patterning was carried out using standard photolithographic techniques and during the etching procedure a sputtered Mo layer was used as a mask. After structuring, Mo leftovers were etched selectively with potassium hexacyanoferrate. This (non-acidic) etchant leaves a surface which proved to be suited for growth. Prior to the next growth procedure the crystal quality of the structured $SrRuO_3$ (primarily the toplayer) was examined. RIE normally leaves an amorphous toplayer which would disturb further epitaxy. Backscattering Kikuchi Diffraction (BKD, a highly surface sensitive technique) in an SEM [16] demonstrated that the $SrRuO_3$ layer was crystalline. After returning the sample into the PLD chamber, an epitaxial PZT layer was grown and subsequently a

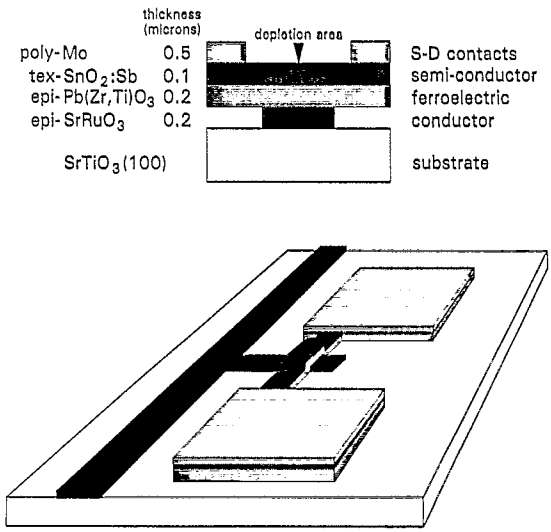

Fig. 9. All-oxide ferroelectric field effect device.

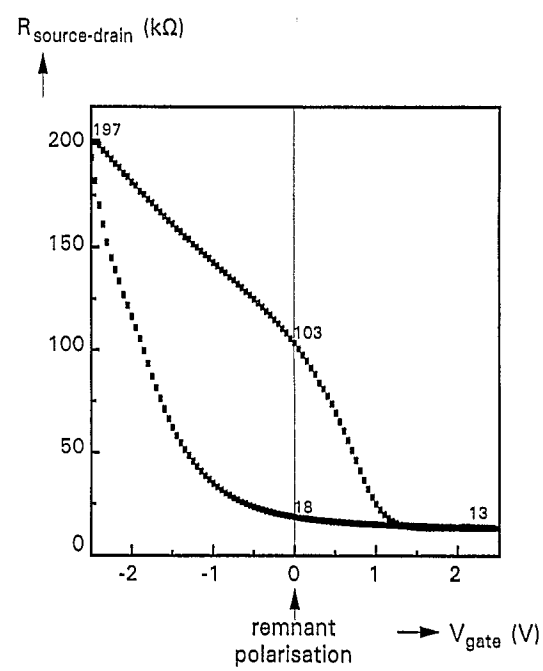

Fig. 10. Electrical characteristic of ferroelectric field effect device: the resistance of the source–drain channel is influenced by the direction of polarisation in the ferroelectric.

[2] The charge carrier concentration was determined using Hall measurements.

layer of SnO_2:Sb. Since SnO_2 exhibits the rutile crystal structure, epitaxy turned out to be impossible on the (100) perovskite orientation of the ferroelectric. For an epitaxial-like growth of SnO_2 the perovskite (111) orientation is necessary [17]. The total stack was structured using the same technique described before. Part of the Mo layer (mask) was used to contact the semiconductor layer (see Fig. 9).

The first results of the devices display an electrical characteristic as shown in Fig. 10. The behaviour of the source–drain resistance versus the gate voltage can be explained as follows. When the electric field applied exceeds the coercive field strength of PZT (in this case at $\approx \pm 1.5$ V) the ferroelectric will be polarised. The sign of the applied field determines the polarisation direction. After the switching pulse, the major part of the polarisation of the ferroelectric is maintained (P_{remnant}) at zero gate-voltage. For the two polarisation states the resistance of the source–drain channel is changed by a factor of 5. The R_{s-d}–V_{gate} loop in Fig. 10 shows an asymmetric behaviour. This is most probably caused by a lowering of the field induced by the change in resistivity of the semiconductor caused by the depletion in the source–drain channel. Moreover the materials in contact with the ferroelectric (source, drain and gate) have different work functions: this also might introduce a shift of the loop [13,18].

Acknowledgements

We would like to thank P. van der Sluis, F. Hakkens and A. De Veirman for XRD, RBS and TEM analyses, H. van Kampen and P.J. van der Zaag for magnetic analyses, M. de Jong, A.J. Geurtsen and X. Croizé for off-axis PLD simulations and M. Kraan and W. Keur for target preparations.

References

[1] P. van der Sluis, Mater. Sci. Forum 166–169 (1994) 141.
[2] P.J. van der Zaag, M.T. Johnson, J.J.M. Ruigrok, C. Bordel and H.J. de Wit, J. Magn. Magn. Mater. 129 (1994) L137.
[3] C.M. Williams, D.B. Chrisey, P. Lubitz, K.S. Grabowski and C.M. Cotell, J. Appl. Phys. 75 (1994) 1676.
[4] H.J. Masterson, J.G. Lunney, J.M.D. Coey and A. Moukarika, J. Magn. Magn. Mater. 115 (1992) 155.
[5] Ferrites, in: J. Smit and H.P.J. Wijn, Philips Tech. Libr. (1959) p. 156.
[6] L.A.H. van Hoof, unpublished results.
[7] K. Ohta and N. Kobayashi, Jpn. J. Appl. Phys. 3 (1964) 576.
[8] A.E.M. De Veirman, J. Timmers, F.J.G. Hakkens, J.F.M. Cillessen and R.M. Wolf, Philips J. Res. 47 (1993) 185.
[9] H. Tabata, T. Kawai, S. Kawai, O. Murata, J. Fujioka and S.-I. Minakata, Appl. Phys. Lett. 59 (1991) 2354.
[10] R. Ramesh, H. Gilchrist, T. Sands, V.G. Keramidas, R. Haakenaasen and D.K. Fork, Appl. Phys. Lett. 63 (1993) 3592.
[11] C.B. Eom, R.B. Van Dover, J.M. Phillips, D.J. Werder, J.H. Marshall, C.H. Chen, R.J. Cava, R.M. Fleming and D.K. Fork, Appl. Phys. Lett. 63 (1993) 2570.
[12] J.F.M. Cillessen, R.M. Wolf and A.E.M. De Veirman, Appl. Surf. Sci. 69 (1993) 212.
[13] J.F.M. Cillessen, M.W.J. Prins and R.M. Wolf, submitted.
[14] N. Ianno and K. Erington, Rev. Sci. Instr. 63 (1992) 3525.
[15] D.B. Chrisey and G.K. Hubler, Pulsed Laser Deposition of Thin Films (Wiley, New York, 1994) ch. 7, p. 199.
[16] K.Z. Troost, P. van der Sluis and D.J. Gravesteijn, Appl. Phys. Lett. 62 (1993) 1110.
[17] H.L.M. Chang, H. Zhang, Z. Shen and Q. Wang, J. Mater. Res. 9 (1994) 3108.
[18] C. Sudhama, A.C. Campbell, P.D. Maniar, R.E. Jones, R. Moazzami, C.J. Mogab and J.C. Lee, J. Appl. Phys. 75 (1994) 1014.